# Evidence of Mass Ordering of Charm and Bottom Quark Energy Loss in Au+Au Collisions at RHIC

M. S. Abdallah,[5] B. E. Aboona,[57] J. Adam,[6] L. Adamczyk,[2] J. R. Adams,[40] J. K. Adkins,[31] G. Agakishiev,[29] I. Aggarwal,[42] M. M. Aggarwal,[42] Z. Ahammed,[63] A. Aitbaev,[29] I. Alekseev,[3,36] D. M. Anderson,[57] A. Aparin,[29] E. C. Aschenauer,[6] M. U. Ashraf,[12] F. G. Atetalla,[30] G. S. Averichev,[29] X. Bai,[12] V. Bairathi,[55] W. Baker,[11] J. G. Ball Cap,[21] K. Barish,[11] A. Behera,[54] R. Bellwied,[21] P. Bhagat,[28] A. Bhasin,[28] J. Bielcik,[15] J. Bielcikova,[39] I. G. Bordyuzhin,[3] J. D. Brandenburg,[6] A. V. Brandin,[36] X. Z. Cai,[52] H. Caines,[66] M. Calderón de la Barca Sánchez,[9] D. Cebra,[9] I. Chakaberia,[32] P. Chaloupka,[15] B. K. Chan,[10] F-H. Chang,[38] Z. Chang,[6] A. Chatterjee,[12] S. Chattopadhyay,[63] D. Chen,[11] J. Chen,[51] J. H. Chen,[19] X. Chen,[50] Z. Chen,[51] J. Cheng,[59] S. Choudhury,[19] W. Christie,[6] X. Chu,[6] H. J. Crawford,[8] M. Csanád,[17] M. Daugherity,[1] T. G. Dedovich,[29] I. M. Deppner,[20] A. A. Derevschikov,[44] A. Dhamija,[42] L. Di Carlo,[65] L. Didenko,[6] P. Dixit,[23] X. Dong,[32] J. L. Drachenberg,[1] E. Duckworth,[30] J. C. Dunlop,[6] J. Engelage,[8] G. Eppley,[47] S. Esumi,[60] O. Evdokimov,[13] A. Ewigleben,[33] O. Eyser,[6] R. Fatemi,[31] F. M. Fawzi,[5] S. Fazio,[7] C. J. Feng,[38] Y. Feng,[45] E. Finch,[53] Y. Fisyak,[6] A. Francisco,[66] C. Fu,[12] C. A. Gagliardi,[57] T. Galatyuk,[16] F. Geurts,[47] N. Ghimire,[56] A. Gibson,[62] K. Gopal,[24] X. Gou,[51] D. Grosnick,[62] A. Gupta,[28] W. Guryn,[6] A. Hamed,[5] Y. Han,[47] S. Harabasz,[16] M. D. Harasty,[9] J. W. Harris,[66] H. Harrison,[31] S. He,[12] W. He,[19] X. H. He,[27] Y. He,[51] S. Heppelmann,[9] S. Heppelmann,[43] N. Herrmann,[20] E. Hoffman,[21] L. Holub,[15] C. Hu,[27] Q. Hu,[27] Y. Hu,[19] H. Huang,[38] H. Z. Huang,[10] S. L. Huang,[54] T. Huang,[38] X. Huang,[59] Y. Huang,[59] T. J. Humanic,[40] D. Isenhower,[1] M. Isshiki,[60] W. W. Jacobs,[26] C. Jena,[24] A. Jentsch,[6] Y. Ji,[32] J. Jia,[6,54] K. Jiang,[50] X. Ju,[50] E. G. Judd,[8] S. Kabana,[55] M. L. Kabir,[11] S. Kagamaster,[33] D. Kalinkin,[26,6] K. Kang,[59] D. Kapukchyan,[11] K. Kauder,[6] H. W. Ke,[6] D. Keane,[30] A. Kechechyan,[29] M. Kelsey,[65] Y. V. Khyzhniak,[36] D. P. Kikoła,[64] B. Kimelman,[9] D. Kincses,[17] I. Kisel,[18] A. Kiselev,[6] A. G. Knospe,[33] H. S. Ko,[32] L. Kochenda,[36] A. Korobitsin,[29] L. K. Kosarzewski,[15] L. Kramarik,[15] P. Kravtsov,[36] L. Kumar,[42] S. Kumar,[27] R. Kunnawalkam Elayavalli,[66] J. H. Kwasizur,[26] R. Lacey,[54] S. Lan,[12] J. M. Landgraf,[6] J. Lauret,[6] A. Lebedev,[6] R. Lednicky,[29] J. H. Lee,[6] Y. H. Leung,[32] N. Lewis,[6] C. Li,[51] C. Li,[50] W. Li,[47] X. Li,[50] Y. Li,[59] X. Liang,[11] Y. Liang,[30] R. Licenik,[39] T. Lin,[51] Y. Lin,[12] M. A. Lisa,[40] F. Liu,[12] H. Liu,[26] H. Liu,[12] P. Liu,[54] T. Liu,[66] X. Liu,[40] Y. Liu,[57] Z. Liu,[50] T. Ljubicic,[6] W. J. Llope,[65] R. S. Longacre,[6] E. Loyd,[11] T. Lu,[27] N. S. Lukow,[56] X. F. Luo,[12] L. Ma,[19] R. Ma,[6] Y. G. Ma,[19] N. Magdy,[13] D. Mallick,[37] S. L. Manukhov,[29] S. Margetis,[30] C. Markert,[58] H. S. Matis,[32] J. A. Mazer,[48] N. G. Minaev,[44] S. Mioduszewski,[57] B. Mohanty,[37] M. M. Mondal,[54] I. Mooney,[65] D. A. Morozov,[44] A. Mukherjee,[17] M. Nagy,[17] J. D. Nam,[56] Md. Nasim,[23] K. Nayak,[12] D. Neff,[10] J. M. Nelson,[8] D. B. Nemes,[66] M. Nie,[51] G. Nigmatkulov,[36] T. Niida,[60] R. Nishitani,[60] L. V. Nogach,[44] T. Nonaka,[60] A. S. Nunes,[6] G. Odyniec,[32] A. Ogawa,[6] K. Oh,[46] S. Oh,[32] V. A. Okorokov,[36] K. Okubo,[60] B. S. Page,[6] R. Pak,[6] J. Pan,[57] A. Pandav,[37] A. K. Pandey,[60] Y. Panebratsev,[29] P. Parfenov,[36] A. Paul,[11] B. Pawlik,[41] D. Pawlowska,[64] C. Perkins,[8] J. Pluta,[64] B. R. Pokhrel,[56] J. Porter,[32] M. Posik,[56] V. Prozorova,[15] N. K. Pruthi,[42] M. Przybycien,[2] J. Putschke,[65] H. Qiu,[27] A. Quintero,[56] C. Racz,[11] S. K. Radhakrishnan,[30] N. Raha,[65] R. L. Ray,[58] R. Reed,[33] H. G. Ritter,[32] M. Robotkova,[39] O. V. Rogachevskiy,[29] J. L. Romero,[9] D. Roy,[48] L. Ruan,[6] A. K. Sahoo,[23] N. R. Sahoo,[51] H. Sako,[60] S. Salur,[48] E. Samigullin,[3] J. Sandweiss,[66,*] S. Sato,[60] W. B. Schmidke,[6] N. Schmitz,[34] B. R. Schweid,[54] F. Seck,[16] J. Seger,[14] R. Seto,[11] P. Seyboth,[34] N. Shah,[25] E. Shahaliev,[29] P. V. Shanmuganathan,[6] M. Shao,[50] T. Shao,[19] R. Sharma,[24] A. I. Sheikh,[30] D. Y. Shen,[19] S. S. Shi,[12] Y. Shi,[51] Q. Y. Shou,[19] E. P. Sichtermann,[32] R. Sikora,[2] J. Singh,[42] S. Singha,[27] P. Sinha,[24] M. J. Skoby,[45] N. Smirnov,[66] Y. Söhngen,[20] W. Solyst,[26] Y. Song,[66] H. M. Spinka,[4,*] B. Srivastava,[45] T. D. S. Stanislaus,[62] M. Stefaniak,[64] D. J. Stewart,[66] M. Strikhanov,[36] B. Stringfellow,[45] A. A. P. Suaide,[49] M. Sumbera,[39] B. Summa,[43] X. M. Sun,[12] X. Sun,[13] Y. Sun,[50] Y. Sun,[22] B. Surrow,[56] D. N. Svirida,[3] Z. W. Sweger,[9] P. Szymanski,[64] A. H. Tang,[6] Z. Tang,[50] A. Taranenko,[36] T. Tarnowsky,[35] J. H. Thomas,[32] A. R. Timmins,[21] D. Tlusty,[14] T. Todoroki,[60] M. Tokarev,[29] C. A. Tomkiel,[33] S. Trentalange,[10] R. E. Tribble,[57] P. Tribedy,[6] S. K. Tripathy,[17] T. Truhlar,[15] B. A. Trzeciak,[15] O. D. Tsai,[10] Z. Tu,[6] T. Ullrich,[6] D. G. Underwood,[4,62] I. Upsal,[47] G. Van Buren,[6] J. Vanek,[39] A. N. Vasiliev,[44,36] I. Vassiliev,[18] V. Verkest,[65] F. Videbæk,[6] S. Vokal,[29] S. A. Voloshin,[65] F. Wang,[45] G. Wang,[10] J. S. Wang,[22] P. Wang,[50] X. Wang,[51] Y. Wang,[12] Y. Wang,[59] Z. Wang,[51] J. C. Webb,[6] P. C. Weidenkaff,[20] G. D. Westfall,[35] H. Wieman,[32] S. W. Wissink,[26] R. Witt,[61] J. Wu,[12] J. Wu,[27] Y. Wu,[11] B. Xi,[52] Z. G. Xiao,[59] G. Xie,[32] W. Xie,[45] H. Xu,[22] N. Xu,[32] Q. H. Xu,[51] Y. Xu,[51] Z. Xu,[6] Z. Xu,[10] G. Yan,[51] C. Yang,[51] Q. Yang,[51] S. Yang,[47]

Y. Yang,[38] Z. Ye,[47] Z. Ye,[13] L. Yi,[51] K. Yip,[6] Y. Yu,[51] H. Zbroszczyk,[64] W. Zha,[50] C. Zhang,[54] D. Zhang,[12] J. Zhang,[51] S. Zhang,[13] S. Zhang,[19] Y. Zhang,[27] Y. Zhang,[50] Y. Zhang,[12] Z. J. Zhang,[38] Z. Zhang,[6] Z. Zhang,[13] F. Zhao,[27] J. Zhao,[19] M. Zhao,[6] C. Zhou,[19] Y. Zhou,[12] X. Zhu,[59] M. Zurek,[4] and M. Zyzak[18]

(STAR Collaboration)

[1] *Abilene Christian University, Abilene, Texas 79699*
[2] *AGH University of Science and Technology, FPACS, Cracow 30-059, Poland*
[3] *Alikhanov Institute for Theoretical and Experimental Physics NRC "Kurchatov Institute", Moscow 117218, Russia*
[4] *Argonne National Laboratory, Argonne, Illinois 60439*
[5] *American University of Cairo, New Cairo 11835, New Cairo, Egypt*
[6] *Brookhaven National Laboratory, Upton, New York 11973*
[7] *University of Calabria & INFN-Cosenza, Italy*
[8] *University of California, Berkeley, California 94720*
[9] *University of California, Davis, California 95616*
[10] *University of California, Los Angeles, California 90095*
[11] *University of California, Riverside, California 92521*
[12] *Central China Normal University, Wuhan, Hubei 430079*
[13] *University of Illinois at Chicago, Chicago, Illinois 60607*
[14] *Creighton University, Omaha, Nebraska 68178*
[15] *Czech Technical University in Prague, FNSPE, Prague 115 19, Czech Republic*
[16] *Technische Universität Darmstadt, Darmstadt 64289, Germany*
[17] *ELTE Eötvös Loránd University, Budapest, Hungary H-1117*
[18] *Frankfurt Institute for Advanced Studies FIAS, Frankfurt 60438, Germany*
[19] *Fudan University, Shanghai, 200433*
[20] *University of Heidelberg, Heidelberg 69120, Germany*
[21] *University of Houston, Houston, Texas 77204*
[22] *Huzhou University, Huzhou, Zhejiang 313000*
[23] *Indian Institute of Science Education and Research (IISER), Berhampur 760010 , India*
[24] *Indian Institute of Science Education and Research (IISER) Tirupati, Tirupati 517507, India*
[25] *Indian Institute Technology, Patna, Bihar 801106, India*
[26] *Indiana University, Bloomington, Indiana 47408*
[27] *Institute of Modern Physics, Chinese Academy of Sciences, Lanzhou, Gansu 730000*
[28] *University of Jammu, Jammu 180001, India*
[29] *Joint Institute for Nuclear Research, Dubna 141 980, Russia*
[30] *Kent State University, Kent, Ohio 44242*
[31] *University of Kentucky, Lexington, Kentucky 40506-0055*
[32] *Lawrence Berkeley National Laboratory, Berkeley, California 94720*
[33] *Lehigh University, Bethlehem, Pennsylvania 18015*
[34] *Max-Planck-Institut für Physik, Munich 80805, Germany*
[35] *Michigan State University, East Lansing, Michigan 48824*
[36] *National Research Nuclear University MEPhI, Moscow 115409, Russia*
[37] *National Institute of Science Education and Research, HBNI, Jatni 752050, India*
[38] *National Cheng Kung University, Tainan 70101*
[39] *Nuclear Physics Institute of the CAS, Rez 250 68, Czech Republic*
[40] *Ohio State University, Columbus, Ohio 43210*
[41] *Institute of Nuclear Physics PAN, Cracow 31-342, Poland*
[42] *Panjab University, Chandigarh 160014, India*
[43] *Pennsylvania State University, University Park, Pennsylvania 16802*
[44] *NRC "Kurchatov Institute", Institute of High Energy Physics, Protvino 142281, Russia*
[45] *Purdue University, West Lafayette, Indiana 47907*
[46] *Pusan National University, Pusan 46241, Korea*
[47] *Rice University, Houston, Texas 77251*
[48] *Rutgers University, Piscataway, New Jersey 08854*
[49] *Universidade de São Paulo, São Paulo, Brazil 05314-970*
[50] *University of Science and Technology of China, Hefei, Anhui 230026*
[51] *Shandong University, Qingdao, Shandong 266237*
[52] *Shanghai Institute of Applied Physics, Chinese Academy of Sciences, Shanghai 201800*
[53] *Southern Connecticut State University, New Haven, Connecticut 06515*
[54] *State University of New York, Stony Brook, New York 11794*
[55] *Instituto de Alta Investigación, Universidad de Tarapacá, Arica 1000000, Chile*
[56] *Temple University, Philadelphia, Pennsylvania 19122*
[57] *Texas A&M University, College Station, Texas 77843*
[58] *University of Texas, Austin, Texas 78712*

[59] *Tsinghua University, Beijing 100084*
[60] *University of Tsukuba, Tsukuba, Ibaraki 305-8571, Japan*
[61] *United States Naval Academy, Annapolis, Maryland 21402*
[62] *Valparaiso University, Valparaiso, Indiana 46383*
[63] *Variable Energy Cyclotron Centre, Kolkata 700064, India*
[64] *Warsaw University of Technology, Warsaw 00-661, Poland*
[65] *Wayne State University, Detroit, Michigan 48201*
[66] *Yale University, New Haven, Connecticut 06520*

(Dated: November 30, 2021)

Partons traversing the strongly interacting medium produced in heavy-ion collisions are expected to lose energy depending on their color charge and mass. We measure the nuclear modification factors for charm- and bottom-decay electrons, defined as the ratio of yields, scaled by the number of binary nucleon-nucleon collisions, in $\sqrt{s_{\rm NN}} = 200$ GeV Au+Au collisions to $p$+$p$ collisions ($R_{\rm AA}$), or in central to peripheral Au+Au collisions ($R_{\rm CP}$). We find the bottom-decay electron $R_{\rm AA}$ and $R_{\rm CP}$ to be significantly higher than that of charm-decay electrons. Model calculations including mass-dependent parton energy loss in a strongly coupled medium are consistent with the measured data. These observations provide clear evidence of mass ordering of charm and bottom quark energy loss when traversing through the strongly coupled medium created in heavy-ion collisions.

Ultra-relativistic heavy-ion collision experiments at the Relativistic Heavy-Ion Collider (RHIC) and Large Hadron Collider (LHC) are unique in studying the properties of the strong interaction between the fundamental constituents of nature. The underlying theory describing the strong interaction is Quantum Chromodynamics (QCD). Over the past decades, many experimental observations of the distributions of emitted particles in relativistic collisions have provided evidence that a novel QCD state of matter is created composed of deconfined quarks and gluons: the Quark-Gluon Plasma (QGP) [1, 2]. Heavy-flavor hadrons (those containing a charm or bottom quark) in heavy-ion collisions have emerged as essential probes of the QGP because they have a rest mass much larger than the expected QGP temperature. This restricts their production to the initial hard parton scatterings in the collision, and therefore they can carry information about the entire QGP evolution [3, 4].

Heavy quark energy loss in the produced medium is expected to proceed via (quasi-)elastic scatterings with the medium constituents and induced gluon radiation. Elastic scatterings are expected to be the dominant energy loss mechanism at low transverse momentum ($p_{\rm T}$), while gluon radiation dominates at high $p_{\rm T}$ [5, 6]. Parton energy loss ($\Delta E$) in the QGP is expected to follow a hierarchy ordered by parton color charge and mass, *i.e.*, $\Delta E(g) > \Delta E(u,d,s) > \Delta E(c) > \Delta E(b)$ with $g$, $u$, $d$, $s$, $c$, and $b$ denoting gluons, up, down, strange, charm, and bottom quarks, respectively [5, 6]. Useful quantities to study parton energy loss are the nuclear modification factors, $R_{\rm AA}$ and $R_{\rm CP}$. $R_{\rm AA}$ is defined as the particle yields in heavy-ion collisions divided by the respective yields in $p$+$p$ collisions, scaled by the average number of binary nucleon-nucleon collisions ($N_{\rm coll.}$) in heavy-ion collisions. $R_{\rm CP}$ is defined as the ratio of the yield in head-on heavy-ion (central) collisions to the yield in collisions with small nuclear geometric overlap (peripheral), scaled by a factor to account for the different $N_{\rm coll.}$ in each case. An observation of $R_{\rm AA}$ or $R_{\rm CP}$ that is equal to unity would indicate heavy-ion collisions are an incoherent superposition of individual nucleon-nucleon collisions.

It has been observed at the RHIC and LHC that the $R_{\rm AA}$ of charmed hadrons is much less than unity at high $p_{\rm T}$ [7–11], indicating that charm quarks lose significant energy in the QGP medium. It has also been observed [7–9, 11] that, at $p_{\rm T} > 5$ GeV/$c$, the measured values of charm meson and light-flavor hadron $R_{\rm AA}$ are approximately equal. The interpretation of this observation is difficult due to the interplay of other effects not related to medium induced energy-loss, for example differences in the fragmentation functions and $p_{\rm T}$ spectra [12]. Similarly, the $R_{\rm AA}$ of bottom and charm hadrons are observed to be similar within uncertainties for $p_{\rm T}$ larger than 7 GeV/$c$ at the LHC [11, 13], where differences due to mass effects become small. Measurements at the LHC of non-prompt J/$\psi$ and $D^0$ $R_{\rm AA}$ at $p_{\rm T} < 20$ GeV/$c$ show a hint of energy loss mass ordering when compared to measurements of prompt $D^0$ $R_{\rm AA}$ [14, 15]. However, one needs to take into account the bottom hadron decay kinematics and different heavy-flavor hadron fractions in $p$+$p$ and heavy-ion collisions to interpret the data directly. Models including the mass dependence of parton energy loss have predicted significantly different values of nuclear modification factors for bottom and charm hadrons in heavy-ion collisions in the $p_{\rm T}$ ranges probed at RHIC [16–19]. Therefore, a comparison of charm and bottom hadron nuclear modification factors at RHIC is an excellent probe of the expected hierarchy of parton energy loss.

In this Letter, we report the $R_{\rm AA}$ of electrons from semileptonic decays of open charm and bottom hadrons in Au+Au collisions at $\sqrt{s_{\rm NN}} = 200$ GeV. Additionally, we report the double-ratios of bottom- to charm-decay electron $R_{\rm AA}$ and $R_{\rm CP}$. The Au+Au measurements presented here include the measurement of the inclusive heavy-flavor-decay electron (HFE) spectra and the frac-

tion of bottom-decay electrons to the sum of bottom- and charm-decay electrons $f_b^{AA} \equiv N(b \to e)/N(b + c \to e)$. The data analyzed were recorded by the Solenoidal Tracker At RHIC (STAR) experiment [20] in the years 2014 and 2016.

For the $f_b^{AA}$ measurement, minimum bias (MB) events are selected by requiring a coincidence between the Vertex Position Detectors [21] just outside the beampipe on either end of the STAR detector. There are about 1 billion and 1.1 billion MB events in 2014 and 2016 data, respectively. An additional trigger is used to select high–$p_{\mathrm{T}}$ electrons by selecting events with a single Barrel ElectroMagnetic Calorimeter (BEMC) [22] tower above a transverse energy threshold $E_{\mathrm{T}} > 3.5$ GeV (denoted *high tower* or HT), and this data sample corresponds to an integrated luminosity of 0.2 and 1.0 nb$^{-1}$ in 2014 and 2016 data, respectively. Tracking of charged particles within $|\eta| < 0.7$ is achieved using the Time Projection Chamber (TPC) [23] inside a 0.5 T magnetic field. Track reconstruction and matching to the Heavy Flavor Tracker (HFT) detector [24] is the same as in Ref. [7]. The HFT provides a good track pointing resolution that enables the topological separation of charm- and bottom-decay electrons. The primary vertex (PV) requirements are the same as in Ref. [7]. Particle identification (PID) is conducted using a combination of the TPC, Time-Of-Flight [25], and the BEMC detectors. Additional shower shape information is used in the HT triggered data from the Shower Maximum Detectors (SMD) in the BEMC towers to identify electrons. A projective likelihood multivariate analysis is used to improve the electron purity in the MB sample (see Supplemental Material [26] for details). We additionally reject electron candidates for which we find an oppositely charged electron in the event that produces a di-electron invariant mass less than 0.15 GeV/$c^2$ to reduce backgrounds from light hadron decays and photon conversions (denoted *photonic electrons*). After electron identification requirements, the electron purity is greater than 80% across all measured electron $p_{\mathrm{T}}$ bins. Electron candidates are defined as tracks that pass all the above criteria.

We measure $f_b^{AA}$ in bins of electron $p_{\mathrm{T}}$ by performing a four-component-template likelihood fit to the $\log_{10}$(DCA/cm) distribution of candidate electrons, where the DCA is defined as the distance-of-closest approach of the track projected back to the PV. The hadron templates are taken from a control pion sample. The templates for residual photonic electrons are determined by embedding $\pi^0$, $\eta$, and photon Monte Carlo particles in real data and applying the same selection as data. The normalization for the photonic electron template is constrained to values calculated using a similar procedure as in Ref. [27], and range from 25% to 15% from low to high $p_T$, respectively. The charm- and bottom-decay electron templates are constructed using the data-driven fast simulation technique described in Ref. [7]. All abundant

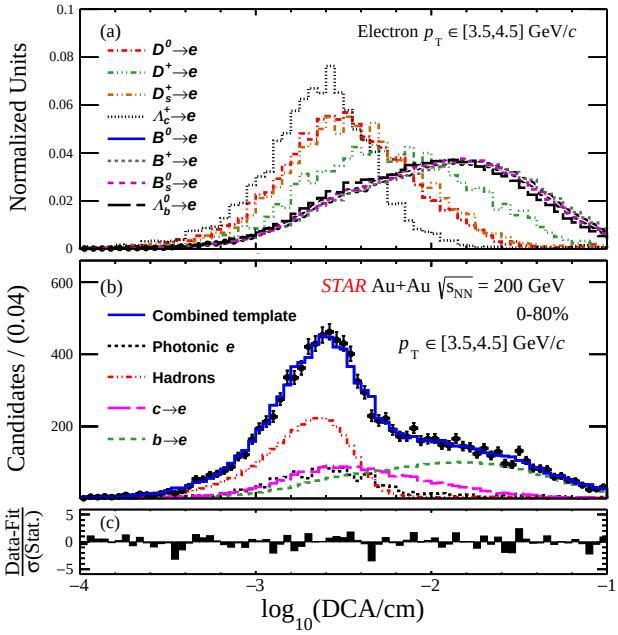


FIG. 1. (a) Decay-electron $\log_{10}$(DCA/cm) distributions for all simulated heavy hadrons with an electron $p_{\mathrm{T}} > 2$ GeV/$c$. (b) Fit to the $\log_{10}$(DCA/cm) of candidate electrons with $p_{\mathrm{T}}$ between 3.5 and 4.5 GeV/$c$ in 2014 data. The solid blue line shows the full template fit, and the various other lines show the individual components. (c) Residual distribution of the template fit scaled by the statistical uncertainties.

ground states are included in the simulation. The initial charm hadron $p_{\mathrm{T}}$ spectra are taken from the measured $D^0$ spectra in Ref. [7], and the relative hadron fractions are from available data [28, 29] or PYTHIA [30]. The bottom hadron spectra are taken from Fixed Order plus Next-to-Leading Logarithms (FONLL) calculations [31, 32], and we assume equal proportions of $B^0$ and $B^+$. The relative $B_s^0$ and $\Lambda_b^0$ fractions are taken from Ref. [33]. We include the contributions from $b \to c \to e$ decays in the bottom-decay electron templates. The decay-electron $\log_{10}$(DCA/cm) distributions for all simulated heavy hadrons with an electron $p_{\mathrm{T}} > 2$ GeV/$c$ are shown in Fig. 1(a). Due to the long and nearly identical bottom hadron lifetimes, we are not systematically sensitive to the bottom relative fractions. Potential backgrounds from Drell-Yan and prompt quarkonia are absorbed in the hadron template, as they produce electrons that point to the PV. Electrons from $K_{e3}$ decays have DCA values outside the fit range considered. An example fit to 2014 data using the described templates is shown in Fig. 1(b), and the residual distribution scaled by the statistical uncertainties in Fig. 1(c).

The invariant yield of inclusive HFE is measured using the same method as in Ref. [27] and utilizes the HT triggered data from the 2014 RHIC Run. One notable difference to Ref. [27] is that the SMD was used to increase the hadron rejection. Compared to the $f_b^{AA}$ analysis, the no-

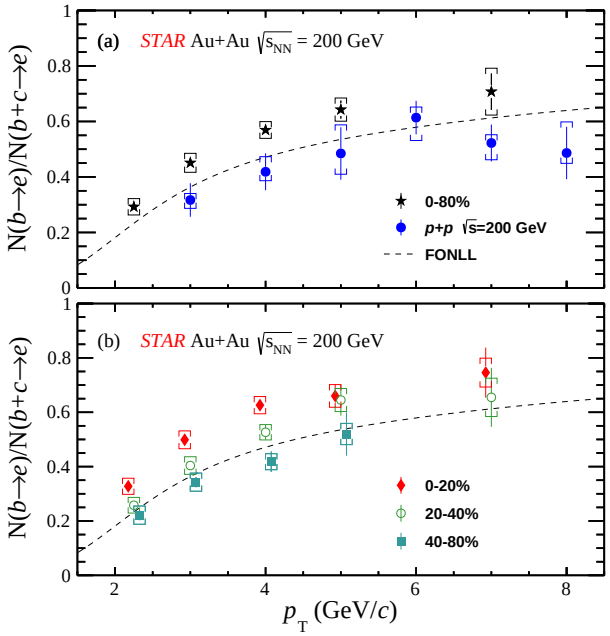


FIG. 2. The measured bottom electron fraction, $f_b^{AA}$, in bins of electron $p_{\rm T}$ in Au+Au collisions at $\sqrt{s_{\rm NN}} = 200$ GeV. (a) shows the full centrality region, and also the measurement of $f_b^{pp}$ in $p$+$p$ collisions at $\sqrt{s} = 200$ GeV [34]. (b) shows $f_b^{AA}$ in three different centrality regions. The error bars show statistical uncertainties, and the brackets show systematic. The dashed line shows the central value of the FONLL prediction [31, 32]. Data points are plotted along the $x$-axis at their respective bin centers, except 0-20% and 40-80% data, which are offset by 75 MeV/$c$ for clarity.

table differences are: 1) the PV is required to be within 30 cm of the center of the STAR detector; and 2) HFT hits are not included in track reconstruction. The inclusive electron yield is first corrected for the mis-identified hadron contamination, which is a 4% subtraction at low $p_{\rm T}$ and 19% at high $p_{\rm T}$. The photonic electron background is then subtracted using a data-driven method where low-mass photonic electron pairs are reconstructed in data and efficiency-corrected to estimate the photonic electron yield. The background-subtracted electron sample is then corrected for the tracking, PID, and trigger efficiencies which are calculated using the embedding technique. Combined, the total efficiency is 5% at low $p_{\rm T}$ and 20% at high $p_{\rm T}$. We finally subtract the electron contributions from quarkonia, vector mesons, and Drell-Yan (see the Supplemental Material [26]). Combined these amount to a ∼20% reduction to the electron yield in the measured $p_{\rm T}$ region. The obtained invariant yield of inclusive HFE can be found in the Supplemental Material [26].

The systematic uncertainties on the inclusive HFE production measurement, which in general increase with increasing $p_{\rm T}$, consist of: 1) the purity uncertainty (2-24%); 2) the photonic electron background uncertainty(16-28%); 3) the reconstruction and PID efficiency uncertainty (3-19%); 4) the trigger efficiency (1-18%); 5) the uncertainty from the quarkonia, vector meson, and Drell-Yan subtraction (1-3%); 6) the relative uncertainty on the $N_{coll.}$ scaling values is 8%. We provide details in the Supplemental Material [26].

The systematic uncertainties on the measured $f_b^{AA}$ fractions are: 1) the uncertainty on the simulated photonic electron cocktail fractions is estimated by varying the relative proportions of photonic conversion electrons and light meson-decay electrons by ∼50%, and ranges from 8% at low $p_{\rm T}$ to less than 1% above 3.5 GeV/$c$; 2) the uncertainty on the residual photonic electron template normalization is estimated by allowing the fit fraction to float by an absolute 5%, and is about 3%; 3) the initial charm hadron $p_{\rm T}$ spectra uncertainty from the measured $D^0$ spectra is about 3%; 4) the $D^+/D^0$ fraction is varied 16%, and is roughly 1–3%; 5) the $\Lambda_c^+/D^0$ fraction is varied using the different models shown in Ref. [29], and is less than 1%; 6) the uncertainty on the electron identification is estimated by tightening the selection, and is 2–3% ; 7) the prior bottom hadron $p_{\rm T}$ spectra uncertainty is estimated by applying both $b \to e$ and $c \to e$ $p_{\rm T}$ suppression calculated in the Duke model [17] described below, and is found to produce a maximum relative deviation of 2.5% that is assigned across all electron $p_{\rm T}$ bins.

The measured values for $f_b^{AA}$ in combined 2014 and 2016 data are shown in Fig. 2(a) for MB collisions, and are compared to $p$+$p$ data [34] and FONLL predictions. The $f_b^{AA}$ fractions are also measured in the 0–20%, 20–40%, and 40–80% centrality regions, where the centralities are defined using the charged particle multiplicity at midrapidity [35], and are related to the impact parameter of the colliding nuclei. 0–20% denotes nuclear collisions with the greatest spacial overlap, while 40–80% denotes peripherally colliding nuclei. These data are shown in Fig. 2(b). A clear centrality dependence is observed, with significantly enhanced $b \to e$ fractions in MB and 0–20% Au+Au collisions compared to $p$+$p$ data and FONLL predictions. The 40–80% data are in good agreement with the $p$+$p$ data.

The inclusive heavy-flavor electron $R_{\rm AA}$ is measured using $p$+$p$ data from Ref. [27] as a baseline, and is shown in Fig. 3(a). We compare to the PHENIX measurement [36] and find the measurements are compatible. We decompose the charm- and bottom-decay $R_{\rm AA}$ using the measured fractions of $f_b$ in Au+Au collisions and $p$+$p$ collisions from Ref. [34]: $R_{\rm AA}^{b\to e} = f_b^{AA}/f_b^{pp} \times R_{\rm AA}^{incl.}$ and $R_{\rm AA}^{c\to e} = (1 - f_b^{AA})/(1 - f_b^{pp}) \times R_{\rm AA}^{incl.}$. For the $p_{\rm T}$ bin 2.5 to 3.5 GeV/$c$, we use the PHENIX inclusive heavy-flavor electron measurement. The charm- and bottom-decay electron $R_{\rm AA}$ values and ratios are shown in Figs. 3(b) and (c), respectively. Note that the ratio measurement does not depend on any absolute $R_{\rm AA}$. The data show that bottom-decay electron $R_{\rm AA}$ compared to charm-

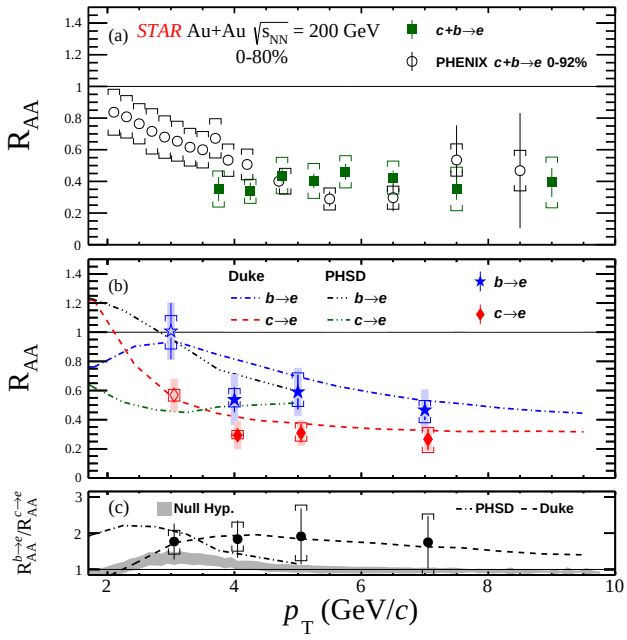


FIG. 3. (a) The measured inclusive heavy-flavor electron $R_{\rm AA}$ (green squares) and the measurement from PHENIX (open circles) [36] in bins of electron $p_{\rm T}$. (b) The measured $R_{\rm AA}$ for bottom- (blue stars) and charm-decay (red diamonds) electrons in bins of electron $p_{\rm T}$. The open markers indicate values calculated using the PHENIX $R_{\rm AA}$ in (a). (c) The $R_{\rm arxivsupplemeAA}$ ratio of bottom- to charm-decay electrons in bins of electron $p_{\rm T}$. In all panels the error bars show statistical uncertainties, and the brackets show systematic. The shaded boxes on the data in (b) show the correlated uncertainty due to the inclusive electron measurement. An 8% global $p$+$p$ luminosity uncertainty is not included in all absolute STAR data. There are additional 8% and 8.1% uncertainties from the $N_{coll.}$ calculations for the absolute STAR and PHENIX data, respectively. The Duke [17] and PHSD [37, 38] models are shown as the various lines in (b) and (c). The null hypothesis calculation is shown in the bottom panel as the gray band. Data points are plotted along the $x$-axis at their respective bin centers, except the charm-decay electron data in (b), which are offset by 50 MeV/$c$ for clarity.

decay electrons are systematically larger, with a central value about 80% larger.

The measured ratios of bottom- and charm-decay electron $R_{\rm CP}$ are shown in Fig. 4 for $R_{\rm CP}(0-20\%/40-80\%)$ and $R_{\rm CP}(0-20\%/20-40\%)$. These data show a more significant deviation from unity because the systematic uncertainties largely cancel in the ratio.

Other mechanisms besides energy loss can lead to the experimental observation of different charm- and bottom-decay electron $R_{\rm AA}$ and $R_{\rm CP}$. A significantly different average parent hadron $p_{\rm T}$ probed within a fixed electron $p_{\rm T}$ bin would produce different suppression values with no mass-dependent energy loss. In simulation we find the average hadron $p_{\rm T}$ is only 12% higher for bottom-decay electrons compared to charm-decay electrons in the measured $p_{\rm T}$ range. Additional effects are due to different ground state hadron fractions in each collision environment and different charm and bottom quark spectra. We assess these effects assuming the same $R_{\rm AA}$ or $R_{\rm CP}$ Duke model curves from the STAR $D^0$ spectra measurement [7] in simulation for charm and bottom hadrons, and propagate to the final state electrons. Initial hadron spectra are taken from [31, 32], with the $\Lambda_{c/b}$ components weighted to match the data in Ref. [33, 39]. In Figs. 3 and 4 these calculations are shown as the shaded bands labeled "Null Hyp.". We performed systematic variations by changing the $D(B)_s$ and $\Lambda_{c(b)}$ fractions by 50% in both $p$+$p$ and Au+Au, and the central $R_{\rm AA}$ and $R_{\rm CP}$ values by a relative 25% in each case. The most significant variation comes from the charm baryon fractions in $p$+$p$ and Au+Au.

We perform a null hypothesis t-test, including data and null hypothesis model uncertainties, with the $R_{\rm AA}$ double ratios in the $p_{\rm T}$ range of 2.5 to 4.5 GeV/$c$, and find a p-value of p = 0.15. The t-test with the $R_{\rm CP}$(0-20%/40-80%) double ratios in the $p_{\rm T}$ range of 2.0 to 4.5 GeV/$c$ yield p = 0.000013, corresponding to a null hypothesis rejection at 4.2 standard deviations. The $R_{\rm CP}$(0-20%/20-40%) double ratio yields a rejection at 3.3 standard deviations. In all t-tests, bin-by-bin correlations of systematic uncertainties in data are included.

We compare our data of charm- and bottom-decay nuclear modification factors to theoretical models describing the heavy-quark dynamics in the de-confined medium in Figs. 3 and 4. The curves denoted "PHSD" show the Parton-Hadron-String-Dynamics model [37, 38] and the "Duke" curves show a modified Langevin transport model [17]. Both models include mass-dependent energy loss mechanisms and the effects described in the null hypothesis calculation above. We find that both models can reproduce the bottom- and charm-decay electron $R_{\rm AA}$ and double ratios of $R_{\rm CP}$.

To summarize, we have measured $R_{\rm AA}$ of inclusive heavy-flavor electrons, and separately for bottom- and charm-decay electrons in the $p_{\rm T}$ range of 2 to 8.5 GeV/$c$ in $\sqrt{s_{\rm NN}}$ = 200 GeV Au+Au collisions. In addition, we have measured the double ratios of bottom- and charm-decay electron $R_{\rm AA}$ and $R_{\rm CP}$. We find the measured values of bottom-decay nuclear modification factors are systematically larger than those of charm-decay electrons after accounting for effects not related to parton energy loss. The significance of this observation, in the $p_{\rm T}$ range of 2 to 4.5 GeV/$c$, is 4.2 and 3.3 standard deviations for the double ratios of $R_{\rm CP}(0-20\%/40-80\%)$ and $R_{\rm CP}(0-20\%/20-40\%)$, respectively. Compared to the data, the Duke and PHSD models are compatible within experimental uncertainties. These observations represent the first significant comparison of bottom and charm hadron energy loss in heavy-ion collisions at RHIC, and provide a clear evidence of mass ordering of charm and bottom quark energy loss when traversing through the strongly coupled medium created in heavy-ion collisions.

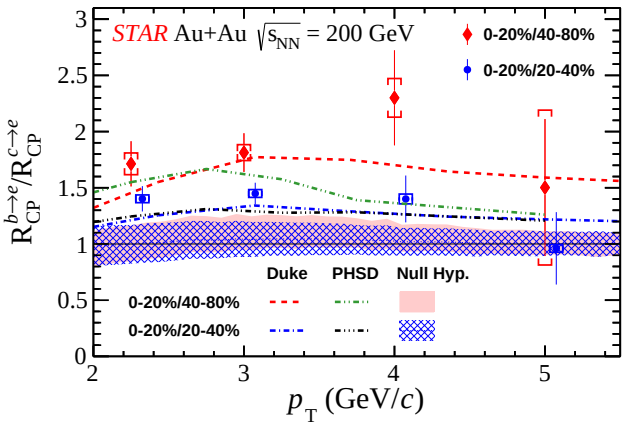


FIG. 4. The measured $R_{\rm CP}$ ratios of bottom-decay electrons to that of charm-decay electrons in $\sqrt{s_{\rm NN}} = 200$ GeV Au+Au data in bins of electron $p_{\rm T}$. The red diamonds show the ratios of $R_{\rm CP}(0-20\%/40-80\%)$, and the blue circles show the ratios of $R_{\rm CP}(0-20\%/20-40\%)$. The error bars and the brackets show statistical and systematic uncertainties, respectively. The Duke [17] and PHSD [37, 38] models are shown as the various lines. The null hypothesis calculations are shown as the shaded bands. $R_{\rm CP}(0-20\%/40-80\%)$ points are plotted along the $x$-axis at their respective bin centers and $R_{\rm CP}(0-20\%/20-40\%)$ is shifted by 75 MeV/$c$ for clarity.

## ACKNOWLEDGEMENTS

We thank the RHIC Operations Group and RCF at BNL, the NERSC Center at LBNL, and the Open Science Grid consortium for providing resources and support. This work was supported in part by the Office of Nuclear Physics within the U.S. DOE Office of Science, the U.S. National Science Foundation, the Ministry of Education and Science of the Russian Federation, National Natural Science Foundation of China, Chinese Academy of Science, the Ministry of Science and Technology of China and the Chinese Ministry of Education, the Higher Education Sprout Project by Ministry of Education at NCKU, the National Research Foundation of Korea, Czech Science Foundation and Ministry of Education, Youth and Sports of the Czech Republic, Hungarian National Research, Development and Innovation Office, New National Excellency Programme of the Hungarian Ministry of Human Capacities, Department of Atomic Energy and Department of Science and Technology of the Government of India, the National Science Centre of Poland, the Ministry of Science, Education and Sports of the Republic of Croatia, RosAtom of Russia and German Bundesministerium für Bildung, Wissenschaft, Forschung and Technologie (BMBF), Helmholtz Association, Ministry of Education, Culture, Sports, Science, and Technology (MEXT) and Japan Society for the Promotion of Science (JSPS).

* Deceased
[1] J. Adams *et al.*, Nucl. Phys. A **757**, 102 (2005).
[2] S. A. Bass, M. Gyulassy, H. Stöcker, and W. Greiner, J. Phys. G: Nucl. Part. Phys. **25**, R1 (1999).
[3] Z. Lin and M. Gyulassy, Phys. Rev. C **51**, 2177 (1995).
[4] M. Cacciari, P. Nason, and R. Vogt, Phys. Rev. Lett. **95**, 122001 (2005).
[5] Y. Dokshitzer and D. Kharzeev, Phys. Lett. B **519**, 199 (2001).
[6] R. Abir *et al.*, Phys. Lett. B **715**, 183 (2012).
[7] J. Adam *et al.* (STAR Collaboration), Phys. Rev. C **99**, 034908 (2019).
[8] B. Abelev *et al.* (ALICE Collaboration), JHEP **2012** (09) 112 (2012).
[9] J. Adam *et al.* (ALICE Collaboration), JHEP **2016** (03) 81 (2016).
[10] S. Acharya *et al.* (ALICE Collaboration), JHEP **2018** (10) 174 (2018).
[11] A. Sirunyan *et al.*, Phys. Lett. B **782**, 474 (2018).
[12] M. Djordjevic, Phys. Rev. Lett. **112**, 042302 (2014).
[13] A. M. Sirunyan *et al.* (CMS Collaboration), Phys. Rev. Lett. **119**, 152301 (2017).
[14] A. M. Sirunyan *et al.*, Eur. Phys. J. C **78**, 509 (2018).
[15] A. M. Sirunyan *et al.* (CMS Collaboration), Phys. Rev. Lett. **123**, 022001 (2019).
[16] H. van Hees, M. Mannarelli, V. Greco, and R. Rapp, Phys. Rev. Lett. **100**, 192301 (2008).
[17] S. Cao, G.-Y. Qin, and S. A. Bass, Phys. Rev. C **92**, 024907 (2015).
[18] P. B. Gossiaux and J. Aichelin, Phys. Rev. C **78**, 014904 (2008).
[19] M. Djordjevic and M. Djordjevic, Phys. Rev. C **90**, 034910 (2014).
[20] K. Ackermann *et al.*, Nucl. Instrum. Meth. A **499**, 624 (2003).
[21] W. Llope *et al.*, Nucl. Instrum. Meth. A **522**, 252 (2004).
[22] M. Beddo *et al.*, Nucl. Instrum. Meth. A **499**, 725 (2003).
[23] M. Anderson *et al.*, Nucl. Instrum. Meth. A **499**, 659 (2003).
[24] G. Contin *et al.*, Nucl. Instrum. Meth. A **907**, 60 (2018).
[25] W. Llope, Nucl. Instrum. Meth. A **661**, S110 (2012).
[26] Supplemental material.
[27] M. S. Abdallah *et al.* (STAR Collaboration), arXiv:2109.13191 .
[28] J. Adam *et al.* (STAR Collaboration), Phys. Rev. Lett. **127**, 092301 (2021).
[29] J. Adam *et al.* (STAR Collaboration), Phys. Rev. Lett. **124**, 172301 (2020).
[30] T. Sjöstrand, S. Mrenna, and P. Skands, Comput. Phys. Commun. **178**, 852 (2008).
[31] M. Cacciari, S. Frixione, N. Houdeau, M. L. Mangano, P. Nason, and G. Ridolfi, JHEP **2012** (1210) 137 (2012).
[32] M. Cacciari, M. L. Mangano, and P. Nason, Eur. Phys. J. C **75**, 610 (2015).
[33] R. Aaij *et al.* (LHCb Collaboration), Phys. Rev. D **100**, 031102 (2019).
[34] M. M. Aggarwal *et al.* (STAR Collaboration), Phys. Rev. Lett. **105**, 202301 (2010).
[35] B. I. Abelev *et al.* (STAR Collaboration), Phys. Rev. C **79**, 034909 (2009).

[36] A. Adare *et al.* (PHENIX Collaboration), Phys. Rev. C **84**, 044905 (2011).
[37] W. Cassing and E. Bratkovskaya, Phys. Rev. C **78**, 034919 (2008).
[38] W. Cassing and E. Bratkovskaya, Nucl. Phys. A **831**, 215 (2009).
[39] S. Acharya *et al.* (ALICE Collaboration), JHEP **2018** (04) 108 (2018).

# Evidence of Mass Ordering of Charm and Bottom Quark Energy Loss in Au+Au Collisions at RHIC: Supplemental Material

(Dated: November 30, 2021)

In the measurement of $f_b^{AA}$, a projective likelihood multivariate analysis (MVA) classifier, analogous to the TMVA method [1], is used to further separate electrons from hadrons in the minimum bias (MB) data sample using probability distribution functions (PDF) of electrons and hadrons in each PID sub-detector. Control samples of electrons and pions are used to determine the PDFs, and are constructed from photonic electrons and $K_s \to \pi^+\pi^-$ decays, respectively, using a tag-and-probe method. The likelihood is calculated as

$$\mathcal{L} = \frac{\prod_i p_i^e}{\prod_i p_i^e + \prod_i p_i^\pi}, \tag{1}$$

where $p_i^{e/\pi}$ are the particle probabilities, and $i$ runs over all PID quantities. Equation 1 is further transformed as $\mathcal{L} \to -1/15 \cdot ln(\mathcal{L}^{-1} - 1)$ to have better discrimination between the signal and background peaks [1]. The variables used in the likelihood classifier are as follows: 1) the track $n\sigma_e$ measured in the TPC, which is defined as $ln[(dE/dx)_m/(dE/dx)_{th}]/\sigma$ with $(dE/dx)_m$ and $(dE/dx)_{th}$ being the measured and expected $dE/dx$ for electrons, respectively, and $\sigma$ being the experimental resolution; 2) the ratio of the track momentum to the energy measured in the largest matched BEMC tower energy; 3) the $\Delta 1/\beta = 1/\beta_{measured} - 1/\beta_e$, where $1/\beta_e$ is the expected value for electrons and $\beta_{measured}$ is that measured by the time-of-flight detector; and 4) the residuals in the $\phi$ and $z$ dimensions of the track projected onto the BEMC cluster center.

The likelihood distribution for electrons and pions with no PID selections are shown in Fig. 1 for 2014 data; similar distributions are observed for 2016 data. An optimization method is performed maximizing the electron purity and corresponds to likelihood selections greater than 0.45 and 0.39 for 2014 and 2016 data, respectively. The hadron fractions before and after the likelihood selection are shown in Fig. 2 for 2014 and 2016 data. It is observed that the likelihood selection has a clear improvement over the standard rectangular selections. There are significant differences between the hadron fractions in 2014 and 2016 data. These are due to the STAR trigger configurations. In 2016, the high-tower triggers were utilized for the majority of data taking and had significant overlap with the minimum bias triggers. Since the high-towers were designed to trigger on electrons in the $p_{\rm T}$ range used for this measurement, and additional particle identification from the shower maximum detectors can then be utilized, most electrons in minimum bias events are re-classified into the high-tower definition of events. In contrast, for 2014 data this was not the case, and the high-tower trigger sample represents a small fraction of the total data set. The efficiencies for the likelihood selections after standard PID selections, determined in the electron control sample, are shown in Fig. 3 for 2014 and 2016 data, and are greater than 87% in the $p_{\rm T}$ range used in this measurement. Therefore, the additional likelihood selection significantly reduces the hadron background without compromising the statistical precision of the signal electron sample.

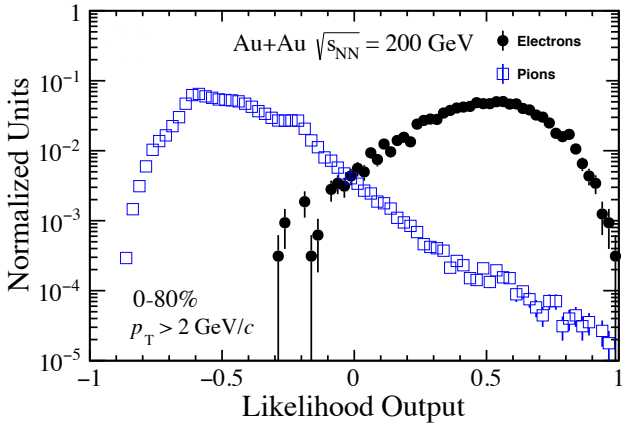


FIG. 1. Likelihood distribution for electrons (black circles) and pions (open blue squares) in 2014 data determined from the data-driven samples described in the text.

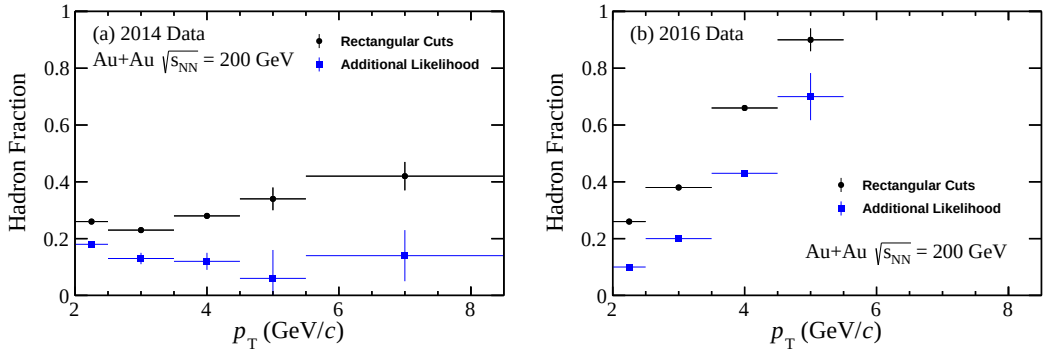


FIG. 2. Hadron contamination for rectangular particle identification (black circles) and with the additional likelihood selection (solid blue squares) in minimum bias data for 2014 (a) and 2016 (b) data respectively.

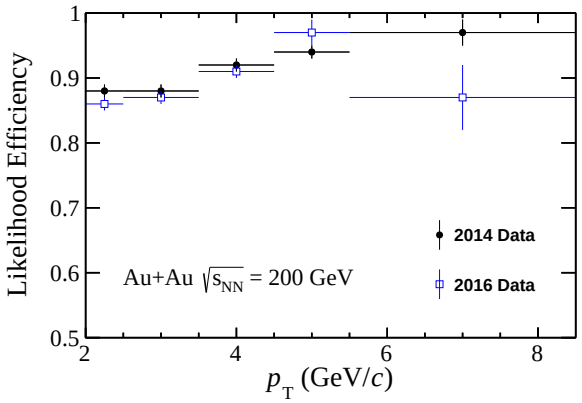


FIG. 3. The likelihood selection efficiency for 2014 (black circles) and 2016 (open blue squares) data.

We subtract the electron contributions from quarkonia, vector mesons, and Drell-Yan in the inclusive HFE measurement. The prompt J/$\psi$ decay background is subtracted using data [2], Fixed Order plus Next-to-Leading Logarithms with Color Evaporation Model calculations [3, 4] and EvtGen [5]. Drell-Yan and Upsilon contributions are subtracted using $N_{coll}$-scaled PYTHIA and EvtGen, respectively, with the former taking no account of the nuclear and shadowing effects and the latter also incorporating the suppression model from [6]. The light-meson decays are estimated using $m_T$-scaling of the $\pi^0$ data [7–9], and PYTHIA and EvtGen. The weak kaon decays ($K_{e3}$) also have a contribution to HFE yield, however, STAR simulation studies find that the $K_{e3}$ contribution is less than 2% at $p_T > 3$ GeV/$c$ in Au+Au collisions at $\sqrt{s_{NN}} = 200$ GeV [10] and thus can be neglected. The obtained invariant yields of these contributions in 0-80% centrality of Au+Au collisions are shown in Fig. 4.

The systematic uncertainties on the inclusive heavy-flavor electron production measurement, which in general increase with increasing $p_T$, are evaluated in a similar procedure as in Ref. [11] and are: 1) the purity uncertainty is estimated based on the uncertainty of the pure electron $dE/dx$ distribution, and is 2-24%; 2) the photonic electron background uncertainty, due to the di-electron efficiency ratio extracted from the embedding samples, is 16-28%; 3) the reconstruction and PID efficiency uncertainty is evaluated by varying the respective selection criteria and is 3-19%; 4) the trigger efficiency uncertainty is evaluated in simulation and is 1-18%; 5) the uncertainty from the quarkonia, vector meson, and Drell-Yan subtraction is due to the uncertainties on the measured spectra and model calculations, and is 1-3%; 6) the relative uncertainty on the $N_{coll.}$ scaling values is 8%.

The invariant yield of inclusive HFE in 0-80% centrality of Au+Au collisions is shown in Fig. 5.

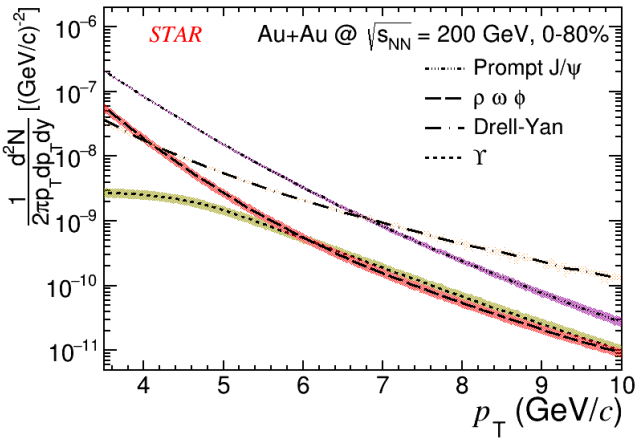


FIG. 4. Invariant yield of the electrons from decays of prompt J/$\psi$ (dot-dashed line), $\Upsilon$ (dotted line), Drell-Yan (long dashdotted line) and light vector mesons (long dashed line) in minimum bias collisions of $\sqrt{s_{\rm NN}}$ = 200 GeV Au+Au data. The bands represent systematic uncertainties.

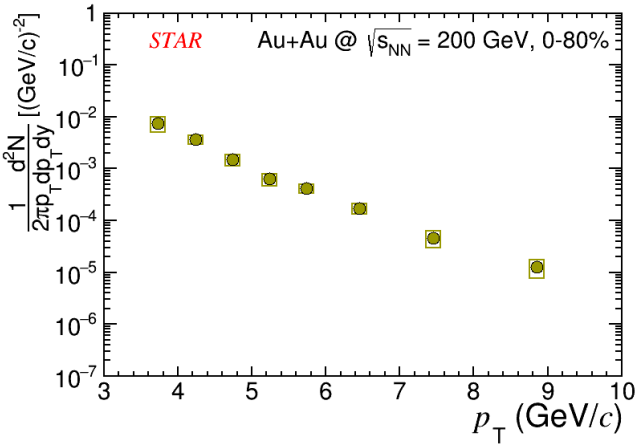


FIG. 5. The HFE invariant yield as a function of $p_{\rm T}$ in minimum bias collisions of $\sqrt{s_{\rm NN}}$ = 200 GeV Au+Au data. The error bars and the boxes represent statistical and systematic uncertainties, respectively.


[1] A. Hocker *et al.*, (2007), arXiv:physics/0703039.
[2] J. Adam *et al.* (STAR Collaboration), Phys. Lett. B **797**, 134917 (2019).
[3] A. Frawley, T. Ullrich, and R. Vogt, Phys. Rept. **462**, 125 (2008).
[4] M. Cacciari, S. Frixione, and P. Nason, JHEP **2001** (03), 006.
[5] D. J. Lange, (2001), BEAUTY2000, Proceedings of the 7th Int. Conf. on B-Physics at Hadron Machines.
[6] B. Krouppa, A. Rothkopf, and M. Strickland, Phys. Rev. D **97**, 016017 (2018).
[7] B. I. Abelev *et al.* (STAR Collaboration), Phys. Rev. Lett. **97**, 152301 (2006).
[8] A. Adare *et al.* (PHENIX Collaboration), Phys. Rev. Lett. **101**, 232301 (2008).
[9] A. Adare *et al.* (PHENIX Collaboration), Phys. Rev. C **87**, 034911 (2013).
[10] L. Adamczyk *et al.* (STAR Collaboration), Phys. Rev. C **95**, 034907 (2017).
[11] M. S. Abdallah *et al.* (STAR Collaboration), arXiv:2109.13191 .